

Supplemental Information

MS # CELL-METABOLISM-D-16-00488R2

Mitchell S.J. et al., Effects of Sex, Strain, and Energy Intake on Hallmarks of Aging in Mice

Index1

Supplemental Experimental Procedures2

Supplemental References9

Supplemental Figures and associated Legends12

Figure S1, related to Figure 2: Binary representation of gene expression related to fatty acid metabolism (A), core components of nucleosome (B), and major urinary proteins (Mup) (C) among all 24 pairwise comparisons.

Figure S2, related to Figure 3: (A) Venn diagrams depicting the impact of CR (treatment), gender, and ‘treatment x gender’ interaction with regard to metabolite accumulation in the liver of B6 and D2 mice. (B) Relative expression of metabolites (e.g., amino acids, lipids, TCA intermediates) in liver of B6 and D2 mice.

Figure S3, related to Figure 4: Metabolites involved in H₂S production in liver (A) and full immunoblot images (B-D).

Figure S4, related to Figure 5: Ubiquitin-proteasome system (A-C) and ultrastructural changes in macroautophagy in response to CR in different mouse strains (D-M).

Figure S5, related to Figure 5: Changes in CMA-related proteins in response to CR in different mouse strains.

Figure S6, related to Figure 6: Effect of CR on mitochondrial properties.

Figure S7, related to Figure 7: Hierarchical clustering of Z-score normalized behavioral, physiological, biochemical and metabolomics data based on values from the different mouse groups.

Supplemental Figures12

Supplemental Tables14

Table S1, related to Figure 1A. Survival statistics for study mice stratified by diet group.

Table S2, related to Figure 1B. Body composition at three time points for study mice stratified by diet group.

Table S3, related to Figure 1E. Necropsy data (S3A) and histopathology data (S3B) -> **Excel sheet.**

Table S4, related to Figure 1F and 1G. Measurement of blood analytes stratified by diet group.

Table S5, related to Figure 2E, 2H. Effect of sex and strain on canonical pathways related to fatty acid metabolism (S5A) and top 20 CR-regulated transcripts (S5B) between the four CR40-CR20 pairwise comparisons. -> **Excel sheet.**

Table S6, related to Figure 3. Two-way ANOVA analysis of the liver metabolomics data.

EXPERIMENTAL PROCEDURES

Survival study. A few mice were censored due to the following reasons: n=6 per group for tissue collection; 1 B6M on 40% CR died before diet started; 1 D2F on AL and 1 D2F on CR died before diets started; 1 D2F on AL died while during a baseline procedure; 3 D2F on 20% CR died before diets started; 2 D2F on 40% CR died before diets started; 1 D2M on AL died before diets started; 2 D2M on 40% CR died before diets started.

Necropsy and gross histopathology at death. All mice that died as part of the study were subject to gross histopathological analysis (n=49-51 per group) and organs were collected and fixed in 4% paraformaldehyde for further analysis. Tissues were stained with hematoxylin and eosin (Histoserv, Germantown, MD) and then scored for pathology by a board certified histopathologist blinded to the treatment group (n=4-12 per study group).

Rectal temperatures. The rectal probe thermometer has an accuracy of 0.1% over the range of -100 to +200 °C. Calibration was performed according to the manufacturer's instructions. For conscious mice, the animals were held gently by the scruff of the neck. The rectal probe was cleansed with isopropanol and then lubricated with petroleum jelly prior to each use. For all temperature measurements, the probe was inserted approximately 1.5 cm into the rectum and allowed to stabilize. The average of three readings in the dark cycle was performed for each mouse.

Determination of serum markers. Glucose was measured in whole blood using the Ascensia Elite glucose meter (Bayer, Mishawaka, IN). Insulin was measured by enzyme-linked immunosorbent assay (ELISA, Crystal Chem, Inc., Downers Grove, IL) according to the kit manufacturers' instructions. Leptin and adiponectin were measured in fasting serum samples with kits according to the manufacturer's instructions (Millipore, Billerica, MA). IGF-1 and IGFBP-1 levels were measured in serum of mice that were fasted for 16-h using an in-house ELISA assay as previously described (Hwang et al., 2008).

Pancreatic islet tissue processing, immunohistochemistry and image analysis. The pancreatic tissue was processed and embedded in paraffin. Pancreatic sections were cut at 5µm thickness using a microtome, and the sections were adhered to poly-L-lysine-coated microscope slides (Thermo Scientific, Philadelphia PA). To obtain a systematic appreciation without bias of the entire pancreas, whole pancreas was sectioned, and every 20th section was saved onto a slide. Pancreatic sections were immunostained according to a previously described protocol (Cai et al., 2014). Briefly, following antigen retrieval with 1× citrate buffer (Biogenex, San Ramon, CA) at 98°C for 20 min, sections were blocked in 5% bovine serum albumin (BSA, Sigma-Aldrich, St-Louis, MO) and 0.1% Tween-20 in 1× Tris-buffered saline (pH 7.4) for 1 h at room temperature. Then tissue was incubated with guinea pig anti-insulin antibody (1:800; Sigma) and mouse anti-glucagon antibody (1:1000; Sigma) overnight in the cold room. After washing, sections were incubated for 1 h in fluorescent secondary antibodies (1:1,000 dilution; Invitrogen, Carlsbad CA) along with 4',6-diamidino-2-phenylindole (1:5,000 dilution; Invitrogen) for nuclear staining. No fluorescent staining was observed in any sections when the primary antibodies were omitted. Sections were imaged with an LSM-710 confocal microscope (Carl Zeiss MicroImaging, Thornwood, NY) in single planes.

Quantification of immunohistochemistry images was performed in Matlab (Mathworks, Natwick MA) using novel software in conjunction with Matlab's image processing toolbox, as described previously (Kim et al., 2011; Martin et al., 2009). Intensity readings of each image ranged from 0 to 256, with 256 being the greatest pixel density and hence the highest staining intensity. The region of interest (ROI) was drawn around each islet after background subtraction. The pixels within the ROI boundaries and above the set threshold of 8 were selected, from which actual islet area was calculated. The normalized variance of the ROI was used to calculate an artificial ellipse from which the major and minor axes were determined. The major axis is the longest diameter that can be drawn in the ellipse, and the minor axis is the shortest diameter, both giving an accurate approximation for the range of the actual islet diameter. Islet sizing, alpha cell numbers, alpha cell percentage and beta cell percentage were performed in an unbiased, random fashion. All the quantifications

were verified using our newly developed pancreatic islet analytical software program, Pancreas++ (Chen et al., 2013). n=4-6 animals per experimental group, age 17-23 mo-old, 11-17 mo on dietary intervention.

Microarray Analysis. Total RNA was isolated from mouse liver with Trizol® (Invitrogen) and then hybridized to BD-202-0202 Illumina BeadChips (San Diego CA). Total RNA was quality-controlled using the Agilent Bioanalyzer RNA 6000 Chip (Agilent, Santa Clara, CA), and labeled according to the manufacturer's instructions using the Illumina® TotalPrep™ RNA amplification kit. A total of 750 ng biotinylated aRNA was hybridized to mouse Ref-8v 2BeadChips (Illumina, San Diego, CA). Following posthybridization rinses, arrays were incubated with streptavidin-conjugated Cy3 and scanned using an Illumina BeadStation 500X Genetic Analysis Systems scanner. Hybridization intensity data were extracted from the scanned images using Illumina BeadStudio GenomeStudio software, V2011.1. Raw data were subjected to Z-normalization, as described elsewhere (Cheadle et al., 2003; Lee et al., 2012). Principal component analysis (PCA) was performed on the normalized Z-scores of all of the detectable probes in the samples using DIANE 6.0 software, available from: (http://www.grc.nia.nih.gov/branches/rrb/dna/diane_software.pdf). Significant genes were selected by the z-test < 0.05, false discovery rate < 0.30, as well as z-ratio > 1.5 in both directions and ANOVA p value < 0.05. Parametric analysis of gene set enrichment (PAGE) was analyzed as previously described (Kim and Volsky, 2005). All raw data are available in the Gene Expression Omnibus database (Accession No. GSE81959. n=6 mice per group, 23-24 mo of age, 17-18 mo on dietary intervention.

Real-time quantitative PCR. Total RNA was isolated from tissues using Trizol®. Complementary DNA was reverse-transcribed using the iScript™ cDNA Synthesis Kit (Biorad). The real-time polymerase chain reaction measurement was performed on individual cDNAs by using SYBR green dye to measure duplex DNA formation. The calculation of mRNA expression was performed according to the $\Delta\Delta CT$ method. n=6 mice per group, 23-24 mo-old 17-18 mo on dietary intervention. The primer pair sequences for murine *Cyp2a5*, *Fh1*, *Mdh2* are proprietary from a commercial source (BioRad Laboratories).

Yeast CR experiments. Experiments were carried out in *S. cerevisiae* BY4741(MATa *his3Δ1 leu2Δ0 met15Δ0 ura3Δ0*) wild-type yeast and respective mutant strains. Chronological aging experiments were performed in either **SCD media** (containing 0.17% yeast nitrogen base (BD Diagnostics; without ammonium sulfate and amino acids (aa), 0.5% (NH₄)₂SO₄, 30 mg/L of all amino acids (except 80 mg/liter histidine, 200 mg/liter leucine, 120 mg/liter lysine), 30 mg/L adenine, and 320 mg/L uracil with 2% glucose) or **CR media** (containing 0.17% yeast nitrogen base, 0.5% (NH₄)₂SO₄, all essential aa, 320 mg/L uracil with 0.5% glucose). At the indicated time points cell survival was determined by clonogenicity: Cell cultures were counted with a CASY cell counter (Schärfe System) and 500 cells were plated on YPD agar plates. Subsequently colony forming units were counted (Ruckenstuhl et al., 2014). Alternatively, cell death was measured via propidium iodide staining and subsequent flow cytometry analysis (BD FACSAria (30,000 cells were evaluated)).

Worm studies. The *fem-1(hc17)* and *eat-2(ad465)* strains were obtained from CGC (Caenorhabditis Genetics Center, University of Minnesota, MN). CY303 (*eat-2(ad465);fem-1(hc17)*) double mutant was constructed by standard genetic cross. Lifespan analysis was performed at 25°C; Bristol N2 and *fem-1(hc17)* strains were supplied with vehicle RNAi (L4440) or with specific RNAi supplementation (*fum-1*; *glna-2*, *mdh-2*) as food source. All the RNAi treatments gave around 90% knockdown efficiency as tested by real-time qPCR. From day-5 adulthood, worms were either fed with normal food or no food. The worms' lifespan was followed until their death. The CY303 strain was treated similarly, except the no food condition was omitted and RNAi efficiency was not verified. Around 20-30 L4 stage worms were transferred to each plate for a total of 150-180 animals per condition. The following day was assigned as d0 of adulthood. Animals were scored as dead or alive and transferred every day to fresh plates seeded with *E. coli* OP50 during the fertile period, and then every other day until death. Worms were considered dead when they stopped pharyngeal pumping and were unresponsive to touch. Worms that died because of internal bagging, desiccation due to crawling on the edge of the plates, or gonad extrusion were censored. Lifespan was analyzed using Prism software (La Jolla, CA). Mean, standard deviation of the mean, and P value were calculated using the log-rank test from pooled

population of animals. Kaplan-Meier survival analysis was used to calculate unadjusted survival of pooled worm populations (Arczewska et al., 2013; Fang et al., 2014).

Metabolomics. Liver tissue (4mg) was homogenized in extraction solution by mixing acetonitrile, isopropanol and water in proportions 3:3:2 (JT Baker, Center Valley PA), then vortexed for 45 seconds and then 5 minutes at 4°C. Following centrifugation for 2 minutes at 14,000 rcf, two aliquots of the supernatant (500µL each aliquot) were made for analysis and one for backup. One aliquot was dried via evaporation overnight in the Labconco Centrivap cold trap concentrator (Labconco, Kansas City MO). The dried aliquot was then re-suspended with 500µL 50% acetonitrile (degassed as given), then centrifuged for 2 minutes at 14,000 rcf using the centrifuge Eppendorf 5415. The supernatant was moved to a new Eppendorf tube and again evaporated to dryness. Internal standards (C08-C30, fatty acid methyl esters) were then added and the sample was derivatized by methoxyamine hydrochloride in pyridine and subsequently by N-methyl-N-trimethylsilyltrifluoroacetamide for trimethylsilylation of acidic protons. Data were acquired using the method as described in (Fiehn et al., 2008). Briefly, metabolites were measured using a Restek corporation rtx5Sil-MS column (Restek Corporation; Bellefonte PA; 30 m length x 0.25 mm internal diameter with 0.25µm film made of 95% dimethyl/5% diphenylpolysiloxane) protected by a 10m long empty guard column which is cut by 20cm intervals whenever the reference mixture QC samples indicate problems caused by column contaminations. This sequence of column cuts has been validated by UC Davis Metabolomics Core with no detrimental effects detected with respect to peak shapes, absolute or relative metabolite retention times or reproducibility of quantifications. This chromatography method yields excellent retention and separation of primary metabolite classes (amino acids, hydroxyl acids, carbohydrates, sugar acids, sterols, aromatics, nucleosides, amines and miscellaneous compounds) with narrow peak widths of 2–3s and very good within-series retention time reproducibility of better than 0.2s absolute deviation of retention times. The mobile phase consisted of helium, with a flow rate of 1 mL/min, and injection volume of 0.5µL. The following mass spectrometry parameters were used: a Leco Pegasus IV mass spectrometer with unit mass resolution at 17 spectra s⁻¹ from 80-500 Da at -70 eV for elution of metabolites. As a quality control, for each sequence of sample extractions, one blank negative control was performed by applying the total procedure (i.e. all materials and plastic ware) without biological sample. Result files were transformed by calculating the sum intensities of all structurally identified compounds for each sample (i.e. those signals that had been positively identified in the data pre-processing schema outlined above), and subsequently dividing all data associated with a sample by the corresponding metabolite sum. The resulting data were multiplied by a constant factor in order to obtain values without decimal places. Intensities of identified metabolites with more than one peak (e.g. for the syn- and anti-forms of methoximated reducing sugars) were summed to only one value in the transformed data set. The original non-transformed data set was retained. The general concept of this data transformation is to normalize data to the ‘total metabolite content’, but disregarding unknowns that might potentially comprise artifact peaks or chemical contaminants. n=6 mice per group, 23-24 mo-old, 17-18 mo on dietary intervention.

NAD⁺ measurement. NAD⁺ was measured in mouse liver extracts as previously described (Frederick et al., 2015). Briefly, NAD⁺ was extracted from ~50mg of liver tissue in 0.6M perchloric acid at 4 °C using a TissueLyzer (Qiagen, Valencia CA), 20 Hz for 6 minutes. Lysates were pelleted at 20,000 × g for 10 min at 4 °C and diluted 1:200 in ice-cold 100 mM phosphate buffer, pH 8. For measurement by cycling assay, alkaline lysates were mixed 1:1 (v/v) with ethanol extraction buffer (250 mM KOH, 50% (v/v) EtOH) and heated at 55 °C for 10 min. Lysate supernatants were diluted 1:50 in ice-cold 100 mM phosphate buffer, pH 8. Following extraction, 5 µl of NAD⁺ standards or diluted tissue extracts was combined with 95 µl of cycling mixture (2% ethanol, 100 µg/ml alcohol dehydrogenase, 10 µg/ml diaphorase, 20 µM resazurin, 10 µM flavin mononucleotide, 10 mM nicotinamide, 0.1% BSA in 100 mM phosphate buffer, pH 8.0). The cycling reaction proceeded for 30 min at room temperature, and resorufin accumulation was measured by fluorescence excitation at 544 nm and emission at 590 nm. n=6 mice per study group, 23-24 mo-old, 17-18 mo on dietary intervention.

Hydrogen sulfide measurement. For detection of liver H₂S production capacity, livers were homogenized in passive lysis buffer (Promega, Madison, WI) followed by several rounds of flash freezing/thawing. Protein content and volume were normalized via BCA Kit (Thermo Fisher Scientific, Waltham, MA). 50-300µg of protein was added to a final reaction in 96-well format containing 10mM Cys and 1mM pyridoxal phosphate. 6x4 inch pieces of lead acetate paper were made by soaking 703 size blotting paper (VWR, Radnor, PA) in 20mM lead acetate (Sigma-Aldrich) and then were vacuum-dried before their placement over the 96-well dish and a 1-2 h incubation at 37°C until lead sulfide was detected but not saturated (Hine et al., 2015). Quantification was performed by volume densitometry using ImageJ software and expressed as an arbitrary unit relative to the AL control within each diet and sex group. n=6 mice per group, 23-24 mo-old, 17-18 mo on dietary intervention.

Tissue processing for planimetric and stereological analysis. Livers were perfused *in situ* with erythrocyte-free oxygenated Krebs-Henseleit bicarbonate buffer (95% O₂:5% CO₂, 37°C) until cleared of blood. A section from the left lateral lobe was fixed for electron microscopy using 2% glutaraldehyde–3% paraformaldehyde in 0.1 M sodium cacodylate buffer (0.1 M sucrose, 2 mM CaCl₂) (Mitchell et al., 2011). Samples were post fixed in 1% osmium tetroxide for 1 h at 4°C in the same buffer, dehydrated and then embedded in Embed 812 resin (Electron Microscopy Sciences, Hatfield, PA) through a series of resin gradients to pure resin. Blocks were formed in fresh resin contained in silicon molds, and the resin was allowed to polymerize for 48-72 h at 65°C. Semi-thick sections (0.5-1µm) were obtained in a Reichert Ultracut ultramicrotome and stained with 1% toluidine blue for assessment of general structural preservation and quantification of hepatocyte nuclear size, a well-established marker of aging liver (Gregg et al., 2012), by planimetry using Image J software (NIH, USA). About 800 nuclei from 4 animals per diet were scored. Ultrathin (40-60 nm) sections were stained with uranyl acetate and lead citrate, and then examined on a Jeol JEM1400 electron microscope (Servicio Centralizado de Apoyo a la Investigación, SCAI, University of Córdoba, Spain) by a blinded investigator. Whole hepatocyte micrographs (10 hepatocytes per mouse, 4 mice per group; age 17-23 mo-old, 11-17 months on dietary intervention) were taken at 4,000 x magnification for stereological analysis of mitochondrial abundance (volume density, V_v) following a point analysis method as previously described (Khraiweh et al., 2013). In addition, micrographs at 12,000 x magnification were also taken from randomly selected areas of hepatocyte cytoplasm for planimetric analysis of mitochondrial size and shape. For this purpose, we evaluated 20 micrographs per mouse using Image J software. A detailed description of methods for morphometric assessment of autophagy is given in a separate section (see below).

Isolation of Mitochondria. Mitochondrial isolation was carried out using a mitochondria isolation kit for tissue (catalog #ab110168, Abcam/MitoSciences, Cambridge MA). All steps were performed at 4°C unless otherwise indicated. Briefly, liver tissue (approx. 150-200 mg) was homogenized in ice-cold isolation buffer containing protease inhibitor cocktail (Sigma-Aldrich, catalog #P-8340) using a glass Dounce homogenizer (20-25 strokes). After centrifugation at 1000 × g for 10 min, the supernatant was transferred to a new tube and centrifuged again at 12,000 × g for 15 min to separate cytosol from the crude mitochondrial fraction. The pellet was washed and resuspended in isolation buffer supplemented with protease inhibitor cocktail. Protein concentration was determined using the Bradford assay method (Bio-Rad, catalog #500-0001) according to the manufacturer's protocol.

Samples (10 µg of mitochondrial extract per lane) were separated by SDS-PAGE under reducing conditions and immunoblotted as indicated below. The MitoProfile total OXPHOS rodent WB antibody cocktail (MitoSciences, catalog #ab110413) contains 5 mouse monoclonal antibodies, including NDUFB8 (catalog #ab110242, 20kDa, CI), SDHB (catalog #ab14714, 30kDa, CII), UQCRC2 (catalog #ab14745, 48kDa, CIII), MTCO1 (catalog #ab14705, 40kDa, CIV) and ATP5A (catalog #ab14748, 55kDa, CV). The cocktail was diluted 1:5000 in PBS-T supplemented with 5% BSA. Quantification of the immunoblots was performed by volume densitometry using ImageJ software and normalized to gel staining with Coomassie Blue Staining (SimplyBlue™ SafeStain, Life Technologies), which serves to verify equal protein loading.

Citrate synthase activity. Citrate synthase activity was determined in whole liver extracts by measuring its activity spectrophotometrically at 412nm at 30°C. Liver homogenates were added to buffer containing 0.1 mM 5,5-dithio-*bis*-(2-nitrobenzoic acid) acid, 0.5 mM oxaloacetate, 50 mM EDTA, 0.31 mM acetyl CoA, 5 mM triethanolamine hydrochloride, and 0.1M Tris-HCl, pH 8.1. Citrate synthase activity was expressed as nmol/min per mg of protein.

Malate dehydrogenase 1 (MDH1) activity assay. MDH1 was measured in mitochondrial extracts using the Abcam kit (ab200009) following the manufacturer's instructions.

Gel Electrophoresis and Western blotting. Samples (10 µg of total liver or mitochondrial extract per lane) were separated by SDS-PAGE under reducing conditions and then electrotransferred onto a polyvinylidene fluoride membrane (0.2µm). Membranes were blocked for 1h in PBS-T (10 mM phosphate-buffered saline/0.05% Tween-20) supplemented with 5% BSA, then incubated for 2 h at room temperature or overnight at 4°C with the indicated primary antibodies. The membranes were then incubated with secondary antibodies conjugated with horseradish peroxidase (1:5000 in PBS-T/5% non-fat milk) for 1 h at room temperature. Immunoreactive bands were visualized using ECL Plus Western Blotting Detection System. or (where indicated) immunoblot membranes were stained with Ponceau S and each band was normalized to the total densitometric value of the Ponceau staining for that line. For comparison of samples run in different membranes, each gel contained a constant line loaded with the same amount of protein from the same sample. This line was used to normalize the final densitometric values across immunoblot membranes and after normalization, B6FAL was given the arbitrary value of 1 and the densitometric intensity of all the other samples was referred to that one in each group of experiments.

The source of the antibodies and dilutions used for immunoblotting were as followed: SIRT1 (Sigma, 1:2500 dilution), PARP-1 (Cell Signaling, 1:500 dilution), SIRT3 (Cell Signaling, 1:1000 dilution), NQO1 (Abcam, 1:2000 dilution), TFAM (Avia Systems Biology, 1:2500 dilution), MDH2 (Abcam, 1:10000 dilution), TXNIP (Medical and Biological Laboratories, 1:1000 dilution), p53 and acetylated p53 (Cell Signaling, 1:1000 dilution for both antibodies), SOD2 and acetylated SOD2 (Abcam, 1:5000 dilution for both antibodies), ACC (Millipore, 1:1000 dilution), PGC-1α (Abcam, 1:1000 dilution), AMPK (Cell Signaling, 1:1000 dilution), FOXO3 (Cell Signaling, 1:1000 dilution), prohibitin (Abcam, catalog #ab28172, 1:600 dilution), and Hsp60 (Abcam, catalog #ab110312, 1:5000 dilution).

Blue native-PAGE. Separation of electron transport chain supercomplexes was performed using Blue native-PAGE protocol as described previously (Wittig et al., 2006). Mitochondrial extracts were solubilized with NativePAGE™ Sample Prep Kit (Life Technologies, catalog #BN2008, Carlsbad CA). Briefly, mitochondria were solubilized in cold 1X NativePAGE™ Sample Buffer containing 2% n-dodecyl-β-D-maltoside and incubated on ice for 15 min. Then, the lysates were centrifuged at 20,000 ×g for 30 min at 4°C, and the supernatants stored at -80°C until use. Protein concentration was determined using the Bradford assay method.

Functional measures of autophagy.

Antibodies. The source of the antibodies and dilutions used for immunoblotting were as followed: LAMP-2A (Invitrogen, # 512200 1:3000), HSC70 (Novus Biologicals, 13D3, 1:5000, Littleton CO), LAMP-1 (University of Iowa Developmental Studies Hybridoma Bank, 1D4B, 1:3000, Iowa City IA), GAPDH (Abcam, 1:3000), LC3 (Cell Signaling, #2775 1:1000), K48-linked ubiquitin (Millipore, #05-1307 1:1000), and K63-linked ubiquitin (Millipore, #05-1308 1:1000).

Subcellular fractionation and isolation of lysosomes. Mouse liver lysosomes were isolated from a light mitochondrial-lysosomal fraction in a discontinuous metrizamide density gradient, and a fraction enriched in the subpopulation of lysosomes active for chaperone-mediated autophagy was further separated by differential centrifugation as previously described (Cuervo et al., 1997). Lysosomal integrity was verified after isolation by measuring β-hexosaminidase activity latency and only preparations with less than 10% broken lysosomes were used (Storrie and Madden, 1990). To obtain cytosolic fractions, the supernatant of the light-mitochondrial-

lysosomal fraction was subjected to centrifugation at 100,000g for 1h at 4°C in a Beckman TL-100 Ultracentrifuge (TLA-100 rotor, Beckman) and the supernatant was collected as the cytosolic fraction.

Proteolysis by intact lysosomes in vitro. Lysosomes isolated from mouse livers were incubated with radiolabeled proteins in 3-(*N*-morpholino) propanesulfonic acid (MOPS) buffer (10 mM MOPS, pH 7.4, 0.3 M sucrose, 1 mM dithiothreitol and 5.4 μM cysteine) for 30 min at 37 °C (Terlecky et al., 1992). Reactions were stopped with 20% TCA and filtered through a Millipore Multiscreen Assay System. Radioactivity in the flow through was detected in a liquid scintillation analyzer (PerkinElmer Wallac, Gaithersburg, MD). Proteolysis was calculated as the percentage of the initial acid-insoluble radioactivity transformed into acid-soluble radioactivity at the end of the incubation.

LC3 flux. To assess LC3 flux in an *ex vivo* setting, livers were harvested, minced and incubated at 37°C for 2h in DMEM with or without lysosomal protease inhibitors (20 mM NH₄Cl and 200 μM leupeptin). Autophagic flux was measured by immunoblot as changes in levels of LC3-II upon inhibition of lysosomal proteolysis (net flux) (Tanida et al., 2005).

Measurement of proteasome activity. Proteasomal catalytic activity was determined using fluorogenic peptides as previously described (Liggett et al., 2010). Briefly, liver homogenates (50 μg protein) were prepared in 0.25M sucrose and diluted 1:2 in reaction buffer. The volume was brought up to 90μl in ice-cold reaction buffer followed by the addition of 10μl of substrate stock solution. Each substrate stock consisted of a 10x solution made in reaction buffer, containing AMC-tagged fluorogenic peptides (Sigma Aldrich) to measure chymotrypsin-like, or peptidyl-glutamyl peptide-hydrolyzing proteasome catalytic activities. Plates were incubated at 37°C for 5 min and fluorescence readings were taken at 15-min intervals using an excitation wavelength of 350nm and an emission of 440nm for 2h. After background correction, fluorescence units were converted to moles of free AMC, using a standard curve. Where indicated, the proteasome inhibitor MG115 (30 μM) was added 30 min prior to the addition of the fluorogenic substrates to determine the contribution of proteasome activity to the cleavage of the fluorescent peptides.

Quantifications of EM pictures. Morphometric analysis was performed in micrographs by two blinded individuals and mean values from both readings were used. Autophagosomes were identified as double membrane vesicles with identifiable cargo and comparable density to the surrounded cytosol. Autolysosomes were denoted as single membrane vesicles containing non-identifiable cargo of density lower than the surrounded cytosol and fragmented organelles. Morphometric profiles compatible with enhanced lipophagy were identified as lipid droplets with increased abundance of membranous structures (often polarized as described before (Singh et al., 2009)). Areas of vesicles and cytosol were measured using manual tracking with Image J software.

Data analysis. Unsaturated images of immunoblotted membranes were captured in the Fujifilm LAS-3000 Imager and densitometric quantification was performed using ImageJ software. All numerical results are reported as mean ± standard error of the mean (s.e.m.) and represent data from a minimum of three independent experiments unless otherwise stated. Statistical significance of the difference between experimental groups in instances of single comparisons was determined by the two-tailed unpaired Student's t-test.

REFERENCES

Arczewska, K.D., Tomazella, G.G., Lindvall, J.M., Kassahun, H., Maglioni, S., Torgovnick, A., Henriksson, J., Matilainen, O., Marquis, B.J., Nelson, B.C., *et al.* (2013). Active transcriptomic and proteomic reprogramming in the *C. elegans* nucleotide excision repair mutant xpa-1. *Nucleic Acids Res.* *41*, 5368-5381.

- Cai, H., Daimon, C.M., Cong, W.N., Wang, R., Chirdon, P., de Cabo, R., Seigny, J., Maudsley, S., and Martin, B. (2014). Longitudinal analysis of calorie restriction on rat taste bud morphology and expression of sweet taste modulators. *J. Gerontol. A Biol. Sci. Med. Sci.* *69*, 532-544.
- Cheadle, C., Vawter, M.P., Freed, W.J., and Becker, K.G. (2003). Analysis of Microarray Data Using Z Score Transformation. *J. Mol. Diagn.* *5*, 73-81.
- Chen, H., Martin, B., Cai, H., Fiori, J.L., Egan, J.M., Siddiqui, S., and Maudsley, S. (2013). Pancreas++ : Automated Quantification of Pancreatic Islet Cells in Microscopy Images. *Front. Physiol.* *3*, 482.
- Cuervo, A.M., Dice, J.F., and Knecht, E. (1997). A population of rat liver lysosomes responsible for the selective uptake and degradation of cytosolic proteins. *J. Biol. Chem.* *272*, 5606-5615.
- Fang, E.F., Scheibye-Knudsen, M., Brace, L.E., Kassahun, H., SenGupta, T., Nilsen, H., Mitchell, J.R., Croteau, D.L., and Bohr, V.A. (2014). Defective mitophagy in XPA via PARP-1 hyperactivation and NAD(+)/SIRT1 reduction. *Cell* *157*, 882-896.
- Fiehn, O., Wohlgemuth, G., Scholz, M., Kind, T., Lee, D.Y., Lu, Y., Moon, S., and Nikolau, B. (2008). Quality control for plant metabolomics: reporting MSI-compliant studies. *Plant J.* *53*, 691-704.
- Frederick, D.W., Davis, J.G., Davila, A., Jr., Agarwal, B., Michan, S., Puchowicz, M.A., Nakamaru-Ogiso, E., and Baur, J.A. (2015). Increasing NAD synthesis in muscle via nicotinamide phosphoribosyltransferase is not sufficient to promote oxidative metabolism. *J. Biol. Chem.* *290*, 1546-1558.
- Gregg, S.Q., Gutiérrez, V., Robinson, A.R., Woodell, T., Nakao, A., Ross, M.A., Michalopoulos, G.K., Rigatti, L., Rothermel, C.E., Kamileri, I., *et al.* (2012). A mouse model of accelerated liver aging caused by a defect in DNA repair. *Hepatology* *55*, :609-621.
- Hine, C., Harputlugil, E., Zhang, Y., Ruckenstuhl, C., Lee, B.C., Brace, L., Longchamp, A., Trevino-Villarreal, J.H., Mejia, P., Ozaki, C.K., *et al.* (2015). Endogenous hydrogen sulfide production is essential for dietary restriction benefits. *Cell* *160*, 132-144.
- Hwang, D.L., Lee, P.D., and Cohen, P. (2008). Quantitative ontogeny of murine insulin-like growth factor (IGF)-I, IGF-binding protein-3 and the IGF-related acid-labile subunit. *Growth Horm IGF Res.* *18*, 65-74.
- Khraiwesh, H., Lopez-Dominguez, J.A., Lopez-Lluch, G., Navas, P., de Cabo, R., Ramsey, J.J., Villalba, J.M., and Gonzalez-Reyes, J.A. (2013). Alterations of ultrastructural and fission/fusion markers in hepatocyte mitochondria from mice following calorie restriction with different dietary fats. *J. Gerontol. A Biol. Sci. Med. Sci.* *68*, 1023-1034.
- Kim, W., Doyle, M.E., Liu, Z., Lao, Q., Shin, Y.K., Carlson, O.D., Kim, H.S., Thomas, S., Napora, J.K., Lee, E.K., *et al.* (2011). Cannabinoids inhibit insulin receptor signaling in pancreatic beta-cells. *Diabetes* *60*, 1198-1209.
- Kim, S.Y., and Volsky, D.J. (2005). PAGE: Parametric analysis of gene set enrichment. *BMC Bioinformatics* *6*, 144.
- Lee, J.S., Ward, W.O., Ren, H., Vallanat, B., Darlington, G.J., Han, E.-S., Laguna, J.C., DeFord, J.H., Papaconstantinou, J., Selman, C., *et al.* (2012). Meta-analysis of gene expression in the mouse liver reveals biomarkers associated with inflammation increased early during aging. *Mech. Ageing Dev.* *133*, 467-478.
- Liggett, A., Crawford, L.J., Walker, B., Morris, T.C., and Irvine, A.E. (2010). Methods for measuring proteasome activity: current limitations and future developments. *Leuk. Res.* *34*, 1403-1409.
- Martin, B., Golden, E., Carlson, O.D., Pistell, P., Zhou, J., Kim, W., Frank, B.P., Thomas, S., Chadwick, W.A., Greig, N.H., *et al.* (2009). Exendin-4 improves glycemic control, ameliorates brain and pancreatic pathologies, and extends survival in a mouse model of Huntington's disease. *Diabetes* *58*, 318-328.

- Mitchell, S.J., Huizer-Pajkos, A., Cogger, V.C., McLachlan, A.J., Le Couteur, D.G., Jones, B., de Cabo, R., and Hilmer, S.N. (2011). Age-Related Pseudocapillarization of the Liver Sinusoidal Endothelium Impairs the Hepatic Clearance of Acetaminophen in Rats. *J. Gerontol. A Biol. Sci. Med. Sci.* 66A, 400-408.
- Ruckenstuhl, C., Netzberger, C., Entfellner, I., Carmona-Gutierrez, D., Kickenweiz, T., Stekovic, S., Gleixner, C., Schmid, C., Klug, L., Sorgo, A.G., *et al.* (2014). Lifespan extension by methionine restriction requires autophagy-dependent vacuolar acidification. *PLoS Genet.* 10, e1004347.
- Singh, R., Kaushik, S., Wang, Y., Xiang, Y., Novak, I., Komatsu, M., Tanaka, K., Cuervo, A.M., and Czaja, M.J. (2009). Autophagy regulates lipid metabolism. *Nature* 458, 1131-1135.
- Storrie, B., and Madden, E. (1990). Isolation of subcellular organelles. *Meth. Enzymol.* 182, 203-225.
- Tanida, I., Minematsu-Ikeguchi, N., Ueno, T., and Kominami, E. (2005). Lysosomal Turnover, but Not a Cellular Level, of Endogenous LC3 is a Marker for Autophagy. *Autophagy* 1, 84-91.
- Terlecky, S.R., Chiang, H.-L., Olson, T.S., and Dice, J.F. (1992). Protein and peptide binding and stimulation of in vitro lysosomal proteolysis by the 73-kDa heat shock cognate protein. *J. Biol. Chem.* 267, 9202-9209.
- Wittig, I., Braun, H.P., and Schagger, H. (2006). Blue native PAGE. *Nat. Protoc.* 1, 418-428.

Supplemental Figures and associated Legends

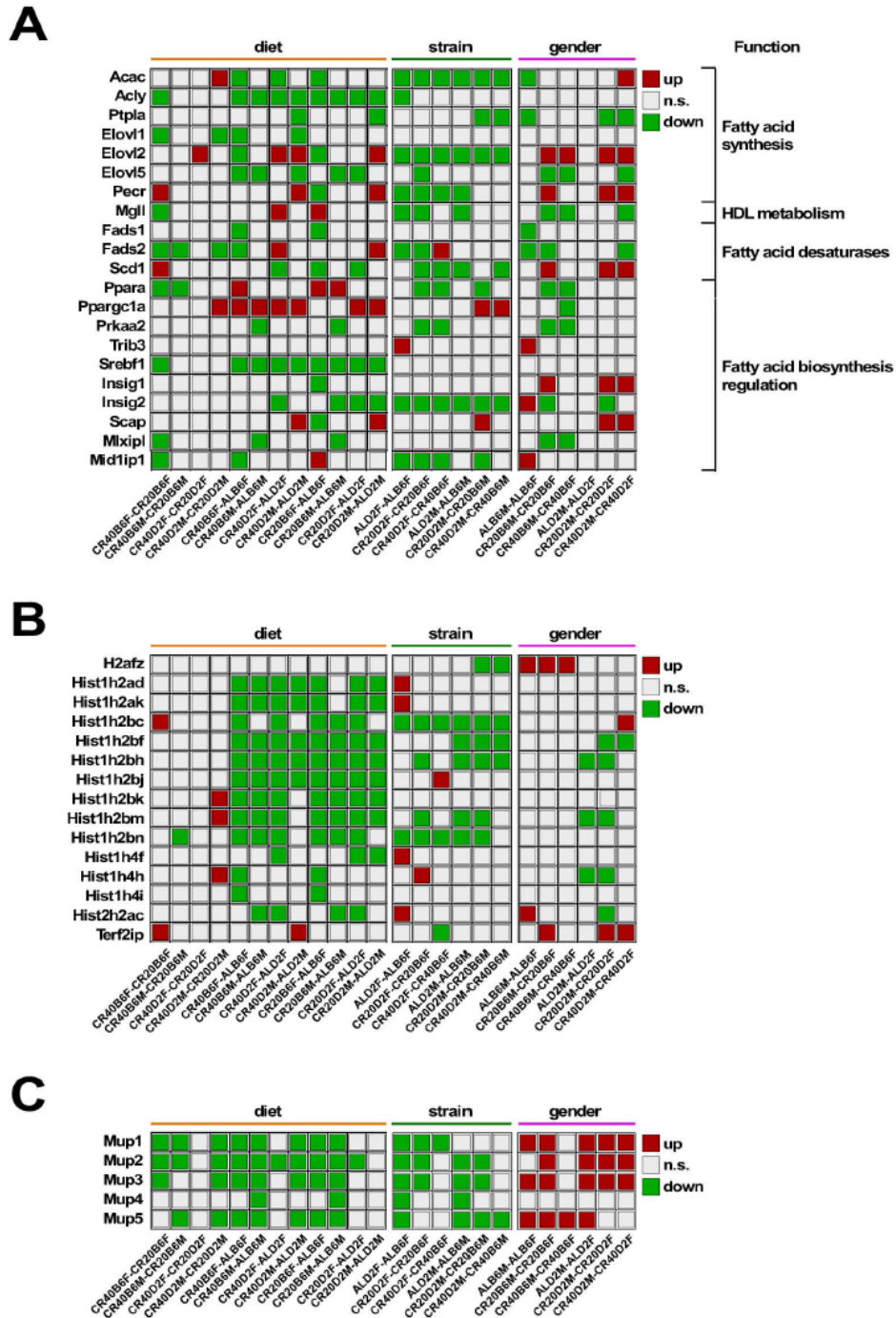


Figure S1, related to Figure 2. Binary representation of gene expression related to fatty acid metabolism (A), core components of nucleosome (B), and major urinary proteins (Mup) (C) among all 24 pairwise comparisons. n.s., non-significant.

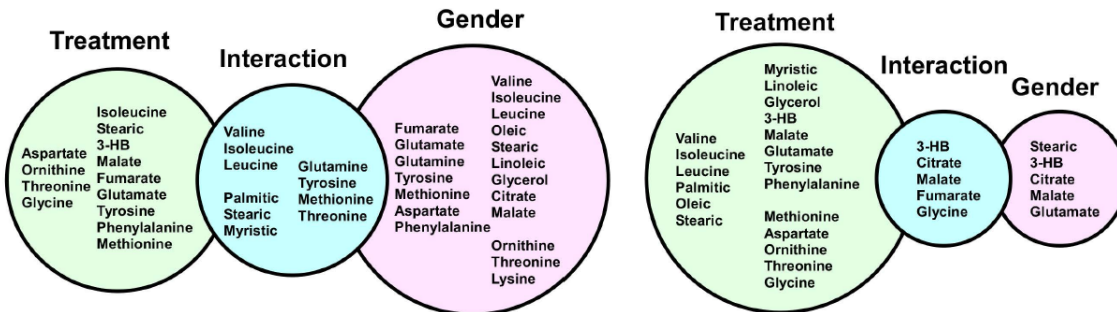
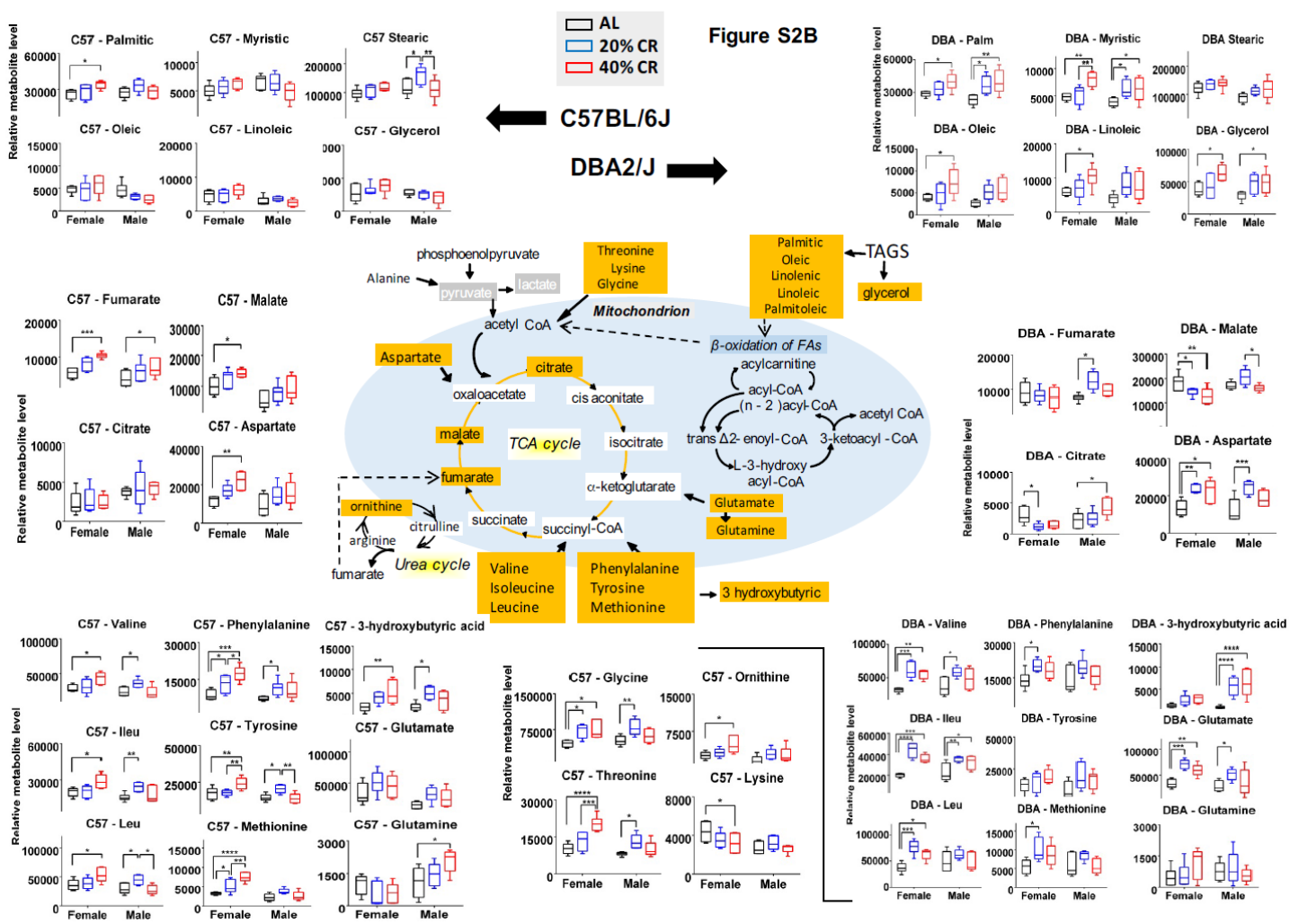
A**B6****D2****B**

Figure S2, related to Figure 3. (A) Venn diagrams depicting the impact of CR (treatment), gender, and ‘treatment x gender’ interaction with regard to metabolite accumulation in the liver of B6 and D2 mice. (B) Relative expression of metabolites (e.g., amino acids, lipids, TCA intermediates) in liver of B6 and D2 mice. All data are n=6 mice per group, 23-24 mo of age, 17-18 mo on diet

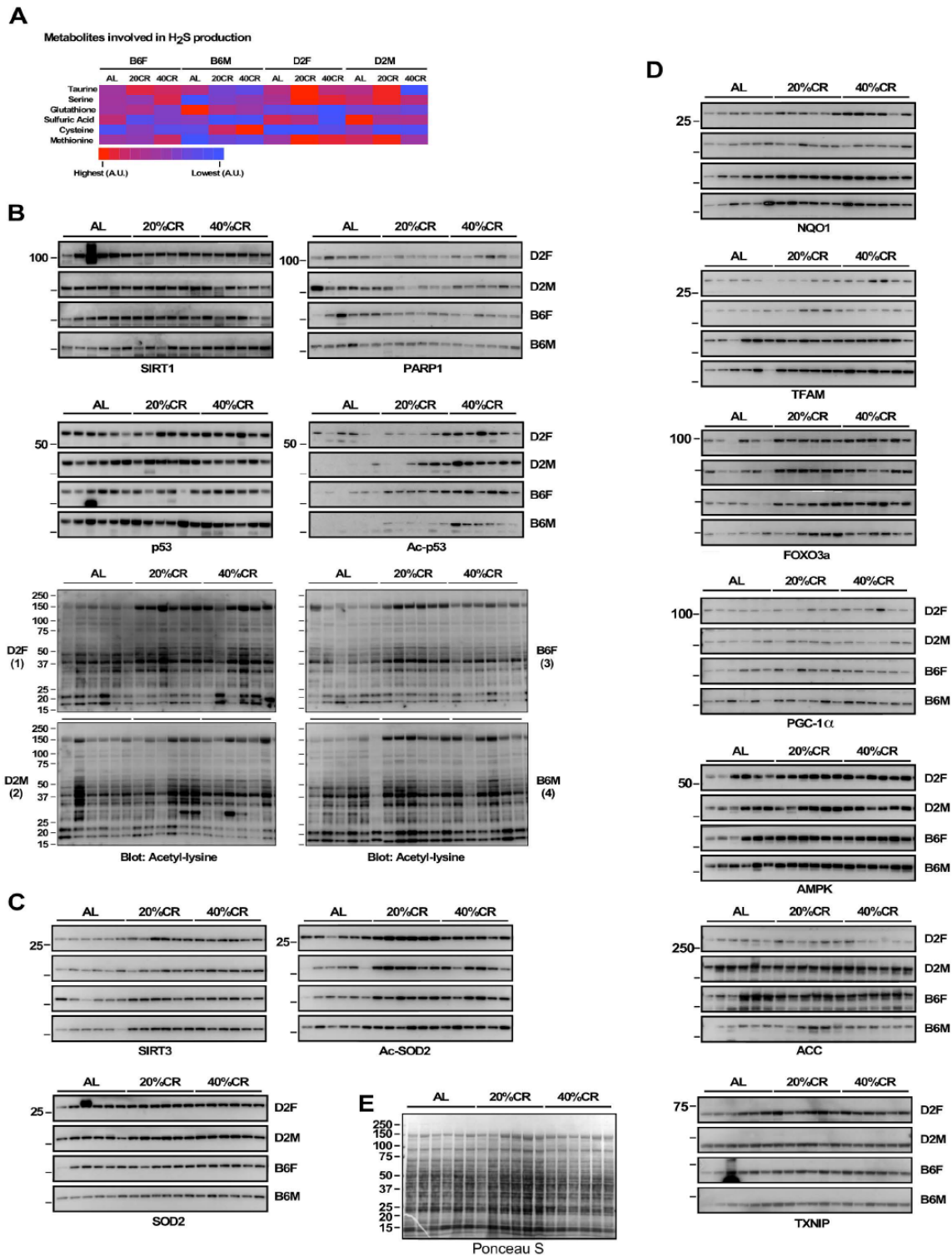


Figure S3, related to Figure 4. (A) Metabolites involved in H₂S production in liver. Heat map of 6 metabolites detected in the liver across the 12 experimental groups (n=6 per group). (B) Full immunoblot images depicting expression levels of SIRT1, PARP1, total and acetylated forms of p53, and protein acetylation. (C) Immunoblots depicting expression levels of SIRT3 as well as acetylated and total forms of SOD2. (D) Immunoblots depicting expression levels of NQO1, PGC-1 α , TFAM, AMPK, FOXO3a, ACC, and TXNIP. (E) Ponceau S staining of a representative blot is shown as loading control. Molecular mass markers (in kDa) are on the left of the immunoblots. All data are n=6 mice per experimental group, 23-24mo age, 17-18mo on diet.

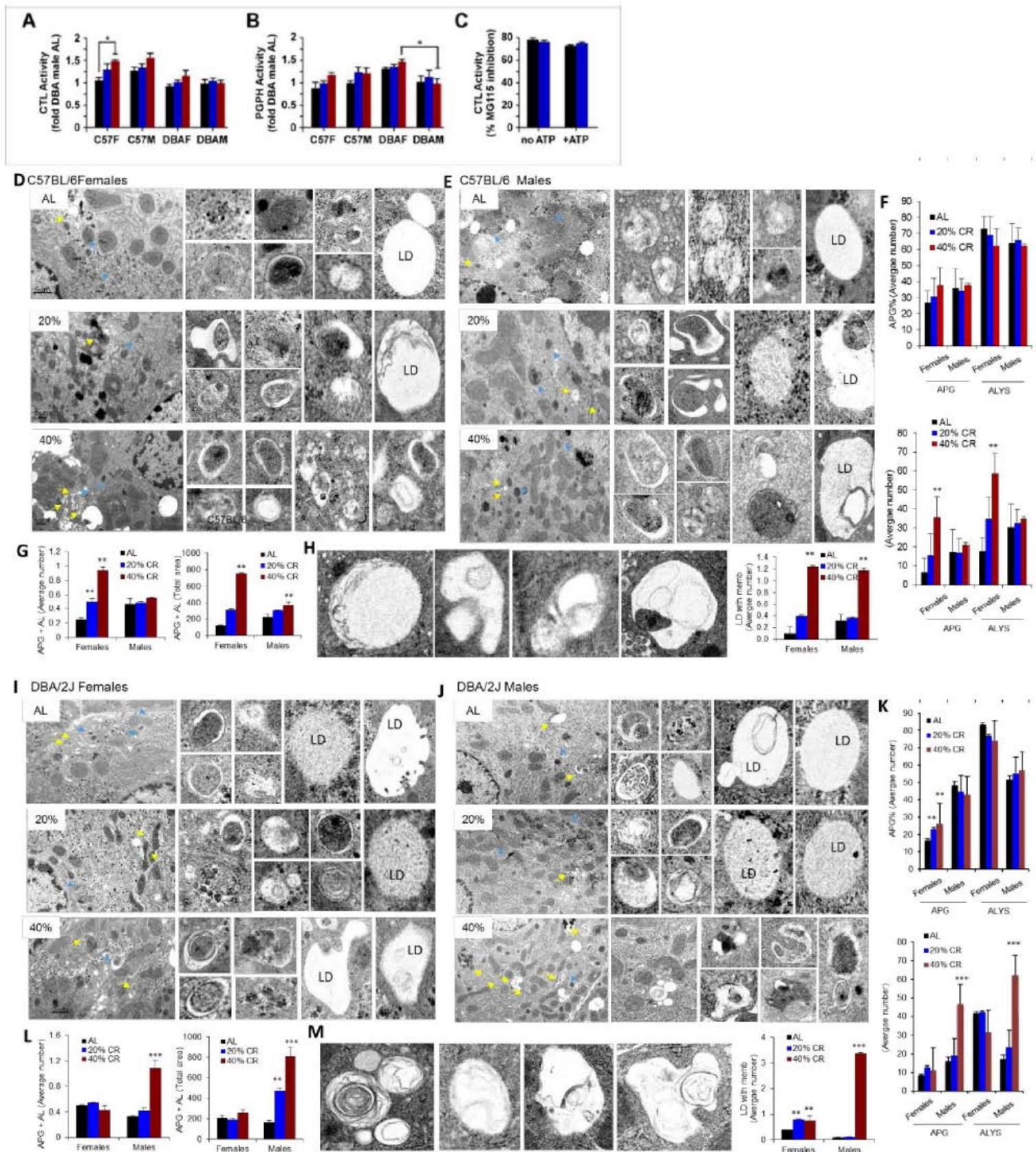


Figure S4, related to Figure 5. Ubiquitin-proteasome system (A-C) and ultrastructural changes in macroautophagy in response to CR in different mouse strains (D-M). (A) Chymotrypsin-like (CTL) and (B) peptidyl-glutamyl peptide-hydrolytic (PGPH) proteasome activity measured in the absence of ATP in liver homogenates. Values are expressed relative to D2 AL males, which were given an arbitrary value of 1. (C) Percentage of inhibition of Chymotrypsin-like

(CTL, *top*) and peptidyl-glutamyl peptide-hydrolytic (PGPH, *bottom*) proteasome activity measured in the absence or presence of ATP after pre-incubation with 30 μ M MG115 for 30 min. n=3. Values are mean + SEM percentage reduction in proteolytic activity following treatment with inhibitors. **(D-G)** Ultrastructural analysis of autophagic compartments. **(D, E, I, J)** Representative transmission electron microscopy images of liver sections of all 12 experimental groups. Inserts show profiles of autophagosomes and autolysosomes and of lipid droplets with features of lipophagy. **(G, L)** Morphometric quantification of average number (left) and total area (right) of autophagic compartments. **(F, K)** Percentage of autophagosomes (APG) and autolysosomes (AL) (top) and average number of each compartment (bottom). **(H, M)** Details of lipid droplet of 40% CR males to show the presence of membranous structures previously described as indicative of lipophagy (left) and quantification of lipophagic structures in each group (right). Quantification of n>10 images per group. All data are mean \pm SEM, n=4-6 biological replicates per experimental group, 17-23mo age, 11-17mo on diet. **p<0.01, ***p<0.001.

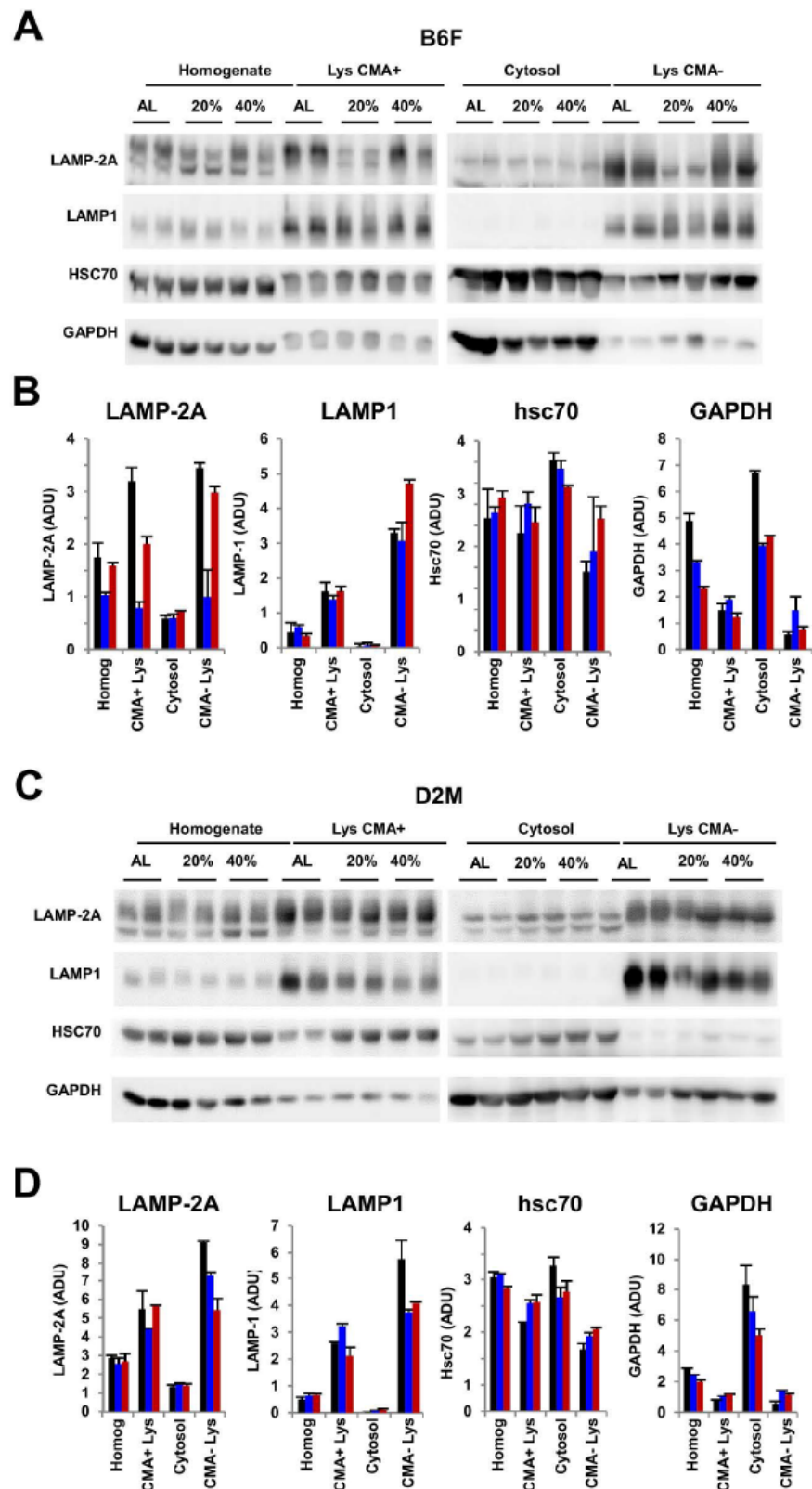


Figure S5, related to Figure 5. Changes in CMA-related proteins in response to CR in different mouse stains. Levels of the main CMA effectors (LAMP-2A and hsc70) and a well-characterized CMA substrate (GAPDH) were compared by immunoblot in the indicated fractions of livers from B6 females (**A, B**) and D2M males (**C, D**). Representative immunoblots are shown in **A** and **C**, and densitometric quantifications upon normalization for a control sample used to standardize values across immunoblots are shown in **B** and **D**. n=2, 17-23mo age, 11-17mo on diet. Values are average and variance.

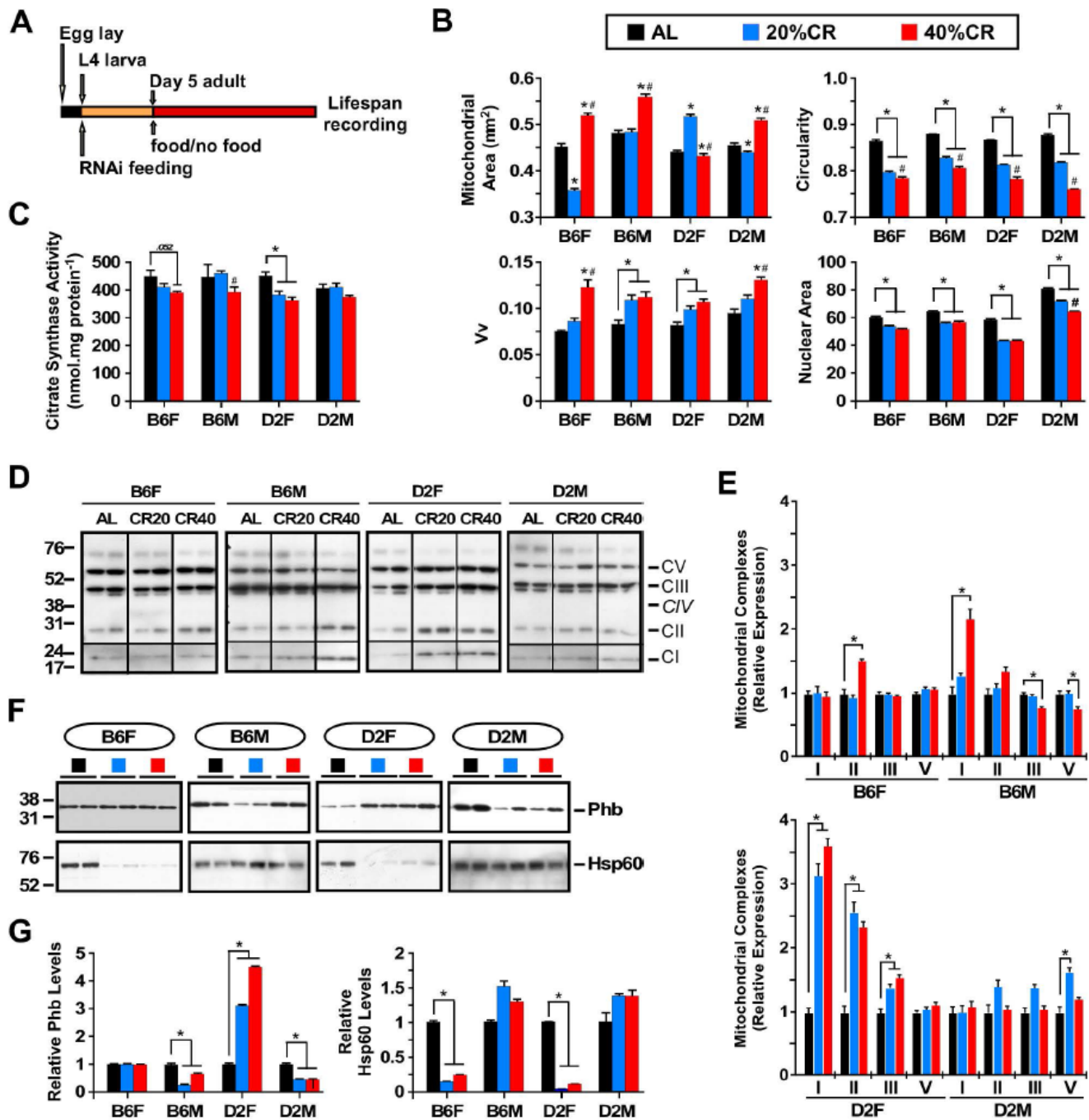


Figure S6, related to Figure 6. Effect of CR on mitochondrial properties. (A) Experimental design used to assess lifespan in *C. elegans*. (B) Ultrastructural properties of hepatocyte mitochondria such as size, circularity, and cell volume fraction occupied by mitochondria (Vv), obtained by transmission electron microscopy, and hepatocyte nuclear size obtained by light microscopy. (C) Citrate synthase activity, n=6 mice per experimental group, 23-24mo age, 17-18mo on diet. (D) Expression levels of intact mitochondrial respiratory chain complexes were determined in liver extracts. Molecular mass markers (in kDa) are on the left of the representative immunoblot (n=6 mice per experimental group, 23-24mo age, 17-18mo on diet). (E) Densitometric quantitation of (E). (F) Total liver lysates were immunoblotted for prohibitin (Phb) and Hsp60 (n=6 mice per experimental group, 23-24mo age, 17-18mo on diet). Membranes were stained with Ponceau S to confirm equal protein loading. (G) Densitometric quantitation of prohibitin (Phb, upper panel) and Hsp60 (lower panel) protein levels after normalization to total protein loaded (e.g., Ponceau S staining of the membranes). Values are expressed relative to AL-fed controls, which were given an arbitrary value of 1. Bars represent mean \pm SEM. *, p<0.05 compared to AL; #, p<0.05 compared to 20% CR.

Table S1, related to Figure 1A. Survival statistics for study mice stratified by diet group.

Group	Survival (days)				
	Q1	Mean	Median	Q3	90% (Max)
ALB6F	656	757	785	853	898
CR20B6F	868 ^a (32.3)	1041.6 ^a (37.6)	1096 ^a (39.6)	1197 ^a (40.3)	1261 ^a (40.4)
CR40B6F	632 ^b (-3.7)	724.1 ^b (-4.3)	754 ^b (-3.9)	797 ^b (-6.6)	1017 ^b (13.3)
ALB6M	669	762.2	807	861	897
CR20B6M	838 ^a (25.3)	958 ^a (25.7)	999 ^a (23.8)	1044 ^a (21.3)	1098 (22.4)
CR40B6M	789 (17.9)	880.8 ^a (15.6)	960 ^a (19.0)	1006 ^a (16.8)	1023 (14.0)
ALD2F	541	598.5	602	699	745
CR20D2F	637 ^a (17.7)	756.2 ^a (26.3)	790 ^a (31.2)	865 ^a (23.7)	916 ^a (23.0)
CR40D2F	689 ^a (27.4)	773.4 ^a (29.2)	758 ^a (25.9)	861 (23.2)	1023 ^a (37.3)
ALD2M	531	616.5	617	701	781
CR20D2M	545 (2.6)	681.6 (10.6)	697 (13.0)	831 (18.5)	933 ^a (19.5)
CR40D2M	431 (-18.8)	680 (10.5)	713 (15.6)	877 (25.1)	1014 ^a (29.8)

The survival for groups is represented in days with the mean percentage change in survival relative to the AL group indicated in the parentheses. AL, ad libitum; CR20, 20% calorie restriction; 40CR, 40% calorie restriction; B6F, C57BL/6 female; B6M, C57BL/6 male; D2F, DBA2/J female; D2M, DBA2/J male.

^a p < 0.05 compared to AL within same strain and sex

^b p < 0.05 compared to 20% CR within same strain and sex

Table S2, related to Figure 1B. Body composition at three time points for study mice stratified by diet group.

Age	Group	BW (g)	Fat (g)	Lean (g)	Lean (%)	Fat (%)	Lean:Fat
10-14 weeks age	B6F	25.4±1.8	5.0±0.8	14.8±0.9	69.9±1.5	22.6±1.5	3.2±0.2
	B6M	30.3±1.1	6.0±0.5	17.7±0.6	68.4±1.1	23.1±1.2	3.0±2.2
	D2F	19.7±0.6	3.8±0.2	11.3±0.3	68.9±0.6	23.1±0.7	3.0±0.1
	D2M	26.6±1.4	6.4±0.5	14.9±0.7	64.5±0.6	27.4±0.7	2.4±0.1
11-13 mo	ALB6F	31.0±1.2	7.2±0.5	17.3±0.6	65.4±0.8	27.3±0.9	2.4±0.1
	CR20B6F	25.3±0.6 ^a	5.4±0.3 ^a	13.4±0.4 ^a	65.5±0.9	26.2±0.9	2.5±0.1
	CR40B6F	23.8±0.4 ^a	5.6±0.2 ^a	11.8±0.3 ^a	61.4±0.6 ^a	29.2±0.6 ^a	2.1±0.1 ^a
	ALB6M	37.8±2.8	9.0±1.2	21.3±1.4	65.3±1.1	27.1±1.3	2.4±0.2
	CR20B6M	32.5±1.2	6.9±0.3	17.1±0.7 ^a	64.7±0.5	26.2±0.5	2.5±0.1
	CR40B6M	27.8±0.6 ^a	6.3±0.1	14.2±0.3 ^a	62.7±0.3	27.7±0.3	2.3±0.0
	ALD2F	30.0±1.3	6.8±0.6	16.2±0.6	65.5±1.0	27.2±1.1	2.4±0.1
	CR20D2F	24.9±0.7 ^a	5.4±0.2 ^a	12.6±0.4 ^a	63.9±0.4	26.4±0.5	2.3±0.1
	CR40D2F	19.7±0.7 ^a	4.0±0.1 ^a	9.8±0.4 ^a	64.9±0.5	26.4±0.5	2.5±0.1
	ALD2M	36.8±1.1	9.4±0.3	19.9±0.7	62.8±0.6	29.8±0.5	2.1±0.1
	CR20D2M	28.0±2.7 ^a	6.5±0.9 ^a	14.5±1.6 ^a	63.5±0.7	28.0±0.8	2.3±0.1
	CR40D2M	27.5±1.2 ^a	6.5±0.6 ^a	14.1±0.7 ^a	62.2±1.0	28.6±0.9	2.2±0.1
23-24 mo	ALB6F	28.7±1.1	6.5±0.6	18.1±0.1	69.4±0.4	23.1±1.1	3.5±0.0
	CR20B6F	22.7±0.3 ^a	5.2±0.1 ^a	11.5±0.1 ^a	62.6±0.3 ^a	28.3±0.3 ^a	2.2±0.4 ^a
	CR40B6F	17.5±0.8 ^a	3.9±0.2 ^a	9.6±0.2 ^a	64.6±0.7 ^a	26.0±0.7 ^a	2.6±0.1 ^a
	ALB6M	32.9±1.3	10.0±0.9	24.6±1.0	66.6±1.0	25.7±1.1	2.8±0.2
	CR20B6M	30.7±0.8	7.4±0.1 ^a	16.2±0.2 ^a	62.1±0.2 ^a	28.4±0.2 ^a	2.2±0.0 ^a
	CR40B6M	23.9±0.3 ^a	5.5±0.2 ^a	13.0±0.2 ^a	63.3±0.5	27.0±0.4 ^a	2.4±0.0 ^a
	ALD2F	24.9±0.8	3.8±0.6	17.0±0.6	75.5±2.0	16.4±2.1	5.2±0.9
	CR20D2F	20.9±0.7	4.4±0.2	12.0±0.3 ^a	66.8±1.1 ^a	24.2±1.0 ^a	2.9±0.2 ^a
	CR40D2F	18.8±0.6 ^a	3.9±0.1	9.4±0.2 ^a	64.3±0.3 ^a	26.5±0.3 ^a	2.4±0.0 ^a
	ALD2M	28.9±1.0	4.9±0.4	17.0±0.7	71.1±1.1	20.2±1.1	3.7±0.3
	CR20D2M	24.7±0.6 ^a	4.9±0.2	13.6±0.4 ^a	66.7±0.6 ^a	24.1±0.6 ^a	2.8±0.1 ^a
	CR40D2M	19.6±0.4 ^a	4.3±0.1	10.6±0.2 ^a	64.5±0.8 ^a	26.2±0.7 ^a	2.5±0.1 ^a

Data are presented as mean ± SEM with n=5-20 per group depending on age group. AL, ad libitum; CR20, 20% calorie restriction; 40CR, 40% calorie restriction; B6F, C57BL/6 female; B6M, C57BL/6 male; D2F, DBA2/J female; D2M, DBA2/J male.

^a p < 0.05 compared to AL within same strain and sex

^b p < 0.05 compared to 20% CR within same strain and sex

Table S4, related to Figure 1F and 1G. Measurement of blood analytes stratified by diet group.

	IGF-1 (ng/mL)	IGFBP-1 (ng/mL)	Insulin (μmol/L)	Glucose (mg/dL)	HOMA-IR (A.U.)	Adiponectin (μg/mL)	Leptin (ng/mL)
ALDZF	570.3 \pm 44.2	15.1 \pm 1.8	120 \pm 23.2	146 \pm 13	6.9 \pm 1.1	4.1 \pm 0.6	0.4 \pm 0.05
CR20DZF	177.0 \pm 43.5*	191.7 \pm 88.6	51.8 \pm 11.1*	94 \pm 11*	2.0 \pm 0.5*	7.1 \pm 0.8*	0.3 \pm 0.1
CR40DZF	88.0 \pm 24.6*	271.2 \pm 81.3 ^d	59.5 \pm 5.9*	75 \pm 6*	1.8 \pm 0.2*	5.7 \pm 1.2	0.3 \pm 0.09
ALD2M	706 \pm 106.1	19.1 \pm 5.7	137.3 \pm 24.8	136 \pm 18	7.9 \pm 1.9	3.8 \pm 0.7	5.5 \pm 3.1
CR20D2M	359.8 \pm 84.0*	84.4 \pm 63.1	58.2 \pm 12.1*	86 \pm 13*	1.9 \pm 0.9*	6.3 \pm 1.3	0.2 \pm 0.08
CR40D2M	166.8 \pm 30.3*	100.1 \pm 54.4	34.8 \pm 7.3*	71 \pm 5*	1.0 \pm 0.2*	8.5 \pm 1.0*	0.3 \pm 0.07
ALB6F	384.5 \pm 47.4	26.9 \pm 11.5	241 \pm 68	150 \pm 8	14.6 \pm 3.9	10.4 \pm 2.6	13.2 \pm 4.2
CR20B6F	355.7 \pm 34.2	4.2 \pm 2.0	56 \pm 3.1*	105 \pm 7*	2.4 \pm 0.3*	17.2 \pm 1.3	2.2 \pm 0.2*
CR40B6F	203.7 \pm 64.4*	54.5 \pm 23.2 ^c	59 \pm 5.0*	100 \pm 5*	2.5 \pm 0.3*	17.6 \pm 2.6	1.0 \pm 0.4*
ALB6M	530.5 \pm 98.0	39.0 \pm 21.7	495 \pm 116	168 \pm 18	37.0 \pm 9.9	6.0 \pm 1.1	26.0 \pm 10.3
CR20B6M	411.0 \pm 93.6	7.4 \pm 6.2	74 \pm 7.6*	128 \pm 9	4.0 \pm 0.6*	13.5 \pm 3.6	0.6 \pm 0.07*
CR40B6M	289.7 \pm 133.1 ^b	4.0 \pm 2.2	62 \pm 13*	105 \pm 2*	2.7 \pm 0.6*	16.6 \pm 4.2	0.3 \pm 0.1*

* $p \leq 0.05$ compared to AL, within same strain and sex.

One way ANOVA followed by Bonferroni post hoc test.

Data are presented as mean \pm SEM with n=6 per group (23-24mo age, 17-18 months on diet) for all measures except adiponectin where n=8 for ALB6F, CR40B6F, and IGF-1 and IGFBP-1 where n=4 for ALD2M, AL, ad libitum, CR20, 20% caloric restriction, 40CR, 40% caloric restriction, B6F, C57BL/6 female; B6M, C57BL/6 male; D2F, DBA2/J female; D2M, DBA2/J male.

^a $p=0.067$

^b $p=0.075$

^c $p=0.094$

^d $p=0.059$

^e $p=0.093$

Table S6, related to Figure 3. Two-way ANOVA analysis of the liver metabolomics data.

Metabolite	Level of significance (p value)					
	Treatment (% of CR)		Sex (Male/Female)		Interaction	
	D2	B6	D2	B6	D2	B6
Valine	< 0.0001	NS	NS	<0.05	NS	<0.01
Isoleucine	<0.0001	<0.05	NS	<0.05	NS	<0.01
Leucine	<0.001	NS	NS	<0.05	NS	<0.01
Palmitic	<0.001	NS	NS	NS	NS	<0.05
Oleic	<0.01	NS	NS	<0.01	NS	NS
Stearic	<0.05	<0.05	<0.01	<0.05	NS	<0.05
Myristic	<0.001	NS	NS	NS	NS	<0.05
Linoleic	<0.01	NS	NS	<0.001	NS	NS
Glycerol	<0.01	NS	NS	<0.05	NS	NS
3-Hydroxybutyric	<0.0001	<0.001	<0.001	NS	<0.05	NS
Citrate	NS	NS	<0.05	<0.01	<0.01	NS
Malate	<0.01	<0.01	<0.01	<0.0001	<0.01	NS
Fumarate	NS	<0.001	NS	<0.01	<0.05	NS
Glutamate	<0.0001	<0.05	<0.01	<0.001	NS	NS
Glutamine	NS	NS	NS	<0.001	NS	<0.05
Tyrosine	<0.05	<0.05	NS	<0.01	NS	<0.001
Phenylalanine	<0.01	<0.001	NS	<0.01	NS	NS
Methionine	<0.05	<0.001	NS	<0.0001	NS	<0.001
Aspartate	<0.0001	<0.01	NS	<0.05	NS	NS
Ornithine	<0.05	<0.05	NS	<0.05	NS	NS
Threonine	<0.01	<0.001	NS	<0.001	NS	<0.001
Lysine	NS	NS	NS	<0.01	NS	NS
Glycine	<0.0001	<0.001	NS	NS	<0.01	NS
Significant	19/23	13/23	5/23	19/23	5/23	10/23

CR, calorie restriction; B6, C57BL/6; D2, DBA2/J. NS=non-significant.